Rock Mechanics 10, 125—137 (1978)

Rock Mechanics
Felsmechanik
Mécanique des Roches
© by Springer-Verlag 1978

Chip Formation in Anisotropic Rock

By

N. J. Altiero and D. L. Sikarskie

With 8 Figures

(Received March 23, 1977)

Summary — Zusammenfassung — Résumé

Chip Formation in Anisotropic Rock. In a series of previous papers it was shown that the fracture of brittle materials such as rock subjected to a globally compressive stress field is accompanied by the formation of microdamage regions. Quantitative descriptions of these regions exist for isotropic materials. In the present paper the theory is extended to brittle materials which exhibit anisotropic fracture behavior due to the presence of a preferred prefracture flaw distribution. Results are computed for three orientations of a given flaw distribution and compared with some existing theoretical and experimental isotropic results. A new type of chip formation, not found in the isotropic case, involving multiple initiation sites, is predicted.

Bruchform in anisotropem Gestein. In einer Serie von Arbeiten wurde gezeigt, daß der Bruch von sprödem Material zu dem auch Stein gehört, unter Einfluß eines global kompressiven Spannungsfeldes eine Beschädigung im Mikrobereich aufweist.

Es gibt bisher quantitative Beschreibungen dieser Erscheinung für isotrope Materialien. In der vorliegenden Arbeit wird die Theorie auf spröde Materialien, die anisotropes Bruchverhalten zufolge vorhandener Risse zeigen, erweitert. Berechnungen werden für drei Richtungen von vorhandenen Rissen durchgeführt und mit einigen vorhandenen theoretischen und experimentellen verglichen. Mittels vieler Ansätze wurde eine neue Bruchform, die im isotropen Fall nicht vorkommt, vorausgesagt.

Formation des copeaux pour le cas anisotrope. Dans une série d'articles antérieurs on a montré que la fracture des matériaux fragiles — tels que la roche sujette à un champ d'effort globalement compressif — est accompagnée de la formation des régions de microendommagement. Des descriptions quantitatives de ce région, existent pour les matériaux isotropes. Ici la théorie est étendue aux matériaux fragiles qui exhibent un comportement anisotrope de la fracture par suite d'une distribution préferée des imperfections avant la fracture. Les résultats sont calculés pour trois orientations d'une distribution donnée des imperfections, et sont comparés avec des

résultats actuels théoriques et expérimentaux pour le cas isotrope. On prédit une nouvelle type de la formation des copeaux — pas trouvée dans le cas isotrope — que mise en jeu les sites multiples d'initiation.

Nomenclature: $A_{1,2}$, $B_{1,2}$, $C_{1,2}$, $D_{1,2}$ — constant coefficients in fitted curves of $C(\gamma), \mu(\gamma)$; $C(\gamma)$ — $\bar{\tau}$-intercept of linear fracture envelope for material orientation, γ; E — Young's modulus; $K[\sigma_1, \sigma_2; C(\gamma), \mu(\gamma)]$ — fracture function based on linear envelope; $K[\sigma_1, \sigma_2; S_t(\gamma), S_c(\gamma)]$ — fracture function based on parabolic envelope; L — characteristic length, see Fig. 2; n, m — exponents in fitted curves of $C(\gamma), \mu(\gamma)$; P — characteristic line load, see Fig. 2; p_x, p_y — dimensionless traction components; $S_t(\gamma)$, $S_c(\gamma)$ — tensile, compressive strengths of material at orientation, γ; u_x, u_y — dimensionless displacement components; α_1 — angle between x-axis and direction of maximum principal stress $(-\pi/2 \leq \alpha_1 \leq \pi/2)$; γ — angle between normal to bedding plane and direction of maximum principal stress $(0 \leq \gamma \leq \pi/2)$; Δ — chip depth; γ^G — angle between x-axis and normal to bedding plane $(0 \leq \gamma^G \leq \pi)$; ξ, ξ' — values of γ at which $C(\gamma)$, $\mu(\gamma)$ are minimum; $\mu(\gamma)$ — slope of linear fracture envelope for material orientation, γ; ν — Poisson's ratio; $\bar{\sigma}_{1,2}, \sigma_{1,2}$ — principal, dimensionless principal stresses at a point $(\sigma_1 > \sigma_2)$; $\bar{\sigma}$ — normal stress on a plane; $\bar{\tau}$ — shear stress on a plane.

1. Introduction

The penetration of brittle rock by a mechanical tool can be considered a cyclic, two-phase process [1]. Under penetration by a wedge, for example, the first phase involves crushing of the material in the vicinity of the wedge tip. As the force on the wedge and, hence, the penetration increase, stresses are induced in the surrounding material which are sufficient to cause incipient fracture, fracture growth and finally a chip. Understanding this second (chipping) phase is of major importance in the practical problem of reducing the energy required to remove a unit volume of material (the specific energy), and is the purpose of this analysis.

Although chip formation is a fracture problem, it is not the usual problem posed in linear elastic fracture mechanics. In the usual problem, the relationship between the macroscopic stress field (tensile for mode I) and finite crack geometry is determined for a given material and global geometry such that the crack begins to propagate (usually unstable propagation). In the present problem, the material contains a distribution of microscopic flaws in a macroscopically compressive stress field. Although a mechanistic explanation can be argued [2], the relationship defining the onset of fracture in this situation[1], i. e., the fracture criterion, is empirical.

Other, even more significant, differences exist. In the usual situation, fracture proceeds by propagation of a single crack. In the present problem, the macrofracture which defines the chip propagates somewhat randomly through a growing damage region which is defined by the presence of microflaw coalescence. This region has been quantitatively defined for isotropic materials [2, 3] and verified experimentally for modelling plaster [4, 5]. It is the purpose of the present paper to extend this theory to anisotropic rock.

[1] Actually the onset of microflaw coalescence.

2. Fracture Analysis of Anisotropic Rock

To a first approximation rock can be considered an elastic material filled with microcracks [6]. Due to the globally[2] compressive stress field of interest here, these microcracks tend to close with increasing stress. Two types of anisotropy are possible. The first is in the elastic stress field and occurs for stress values below fracture initiation. Here, it is also important to identify a second (lower) stress state, namely that necessary to close the cracks. Below this, the material may exhibit both non-linearity and anisotropy due primarily to stiffnesses which depend on both load magnitude and direction [6]. Above the crack closure stress state but below fracture initiation, where one is measuring the "intrinsic" properties of the matrix material, many rocks behave nearly isotropically (see, for example, Refs. [7, 8]). Thus, in the present analysis the assumption of elastic isotropy will be made.

The presence of the closed cracks does, however, effect the fracture characteristics. If the cracks are randomly oriented and distributed, then the fracture characteristics are isotropic. If there is a preferred crack distribution, such as occurs, for example, in certain rocks having bedding planes[3], then the fracture characteristics are anisotropic. This anisotropic fracture behavior has been studied and modeled by several authors [9—14]. The mathematical model to be used in the present analysis is that given by McLamore and Gray [13]. This is an extension (more accurate fit of experimental data) of the variable cohesive shear strength model of Jaeger [10].

The Coulomb Mohr fracture criterion is

$$|\bar{\tau}| + \mu\,\bar{\sigma} = C \tag{1}$$

where $\bar{\tau}, \bar{\sigma}$ are the dimensional shear and normal stresses on an interior plane and C, μ are constants. In the case of linear, isotropic fracture μ, C are true constants. In the case of linear, anisotropic fracture C, μ are functions of γ, where γ is the angle between the normal to the bedding plane and the maximum principal stress direction (tensile stresses positive). Following [13], C, μ can be expressed in the form

$$\begin{aligned} C &= A_i - B_i\,[\cos 2\,(\xi - \gamma)]^n \\ \mu &= C_i - D_i\,[\cos 2\,(\xi' - \gamma)]^m \end{aligned} \tag{2}$$

where ξ, ξ' are the values of γ where C, μ are minimum, respectively, and i takes on the value 1 or 2. A_1, B_1, C_1, D_1 are curve fitted to the experimental data over the range $0 \leq \gamma \leq \xi, \xi'$ and A_2, B_2, C_2, D_2 over the range $\xi, \xi' \leq \gamma \leq \pi/2$. Exponents n, m are "anisotropy type" factors which are also fitted to the experimental data. Fig. 1 is such a plot for the Green River Shale which will be used in the present analysis. Two additional fracture

[2] Local stresses in the vicinity of crack tips are, in fact, tensile.

[3] This anisotropy is of the transversely isotropic type.

cases are also important, namely nonlinear isotropic and nonlinear anisotropic. The nonlinear isotropic fracture analysis was developed in Ref. [2], while the nonlinear anisotropic is discussed in the appendix.

Eq. (1) in terms of principal stresses is

$$\mu(\gamma)(\bar{\sigma}_1+\bar{\sigma}_2)+(1+\mu^2(\gamma))^{1/2}(\bar{\sigma}_1-\bar{\sigma}_2)=2\,C(\gamma) \tag{3}$$

Dimensionless stresses are defined as follows

$$\sigma_1=\frac{\bar{\sigma}_1 L}{P}$$

$$\sigma_2=\frac{\bar{\sigma}_2 L}{P} \tag{4}$$

where P, L are defined in Fig. 2. Substituting into Eq. (3) and solving for P/L:

$$P/L=K[\sigma_1, \sigma_2; C(\gamma), \mu(\gamma)]=\frac{2\,C(\gamma)}{\mu(\gamma)(\sigma_1+\sigma_2)+[1+\mu^2(\gamma)]^{1/2}(\sigma_1-\sigma_2)} \tag{5}$$

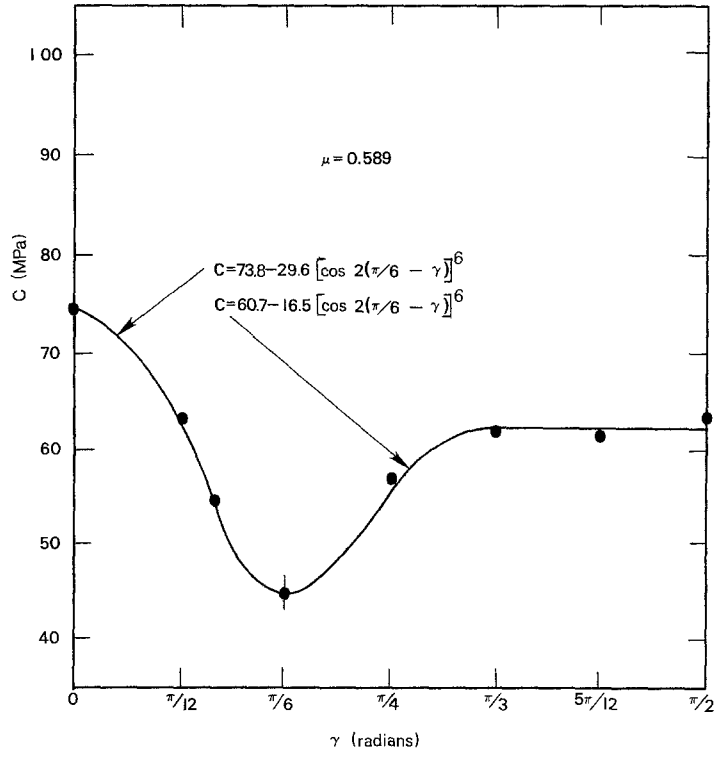

Fig. 1. Variation of C with respect to γ for Green River Shale, as reproduced from McLamore and Gray [13]

Abänderung von C in bezug auf γ für den Green-River-Schiefer (nach McLamore und Iray [13] ermittelt)

Variation de C, étant une fonction de γ, pour l'ardoise Green River (selon McLamore et Iray [13])

Eq. (5) defines a fracture function K. Physically it represents the loading P/L necessary to initiate fracture at that point in the field [2, 3]. In terms of problem solution, K is utilized in the following way. There is a minimum value of $P/L = K_{\min}$ for which fracture is initiated at some point in the field.

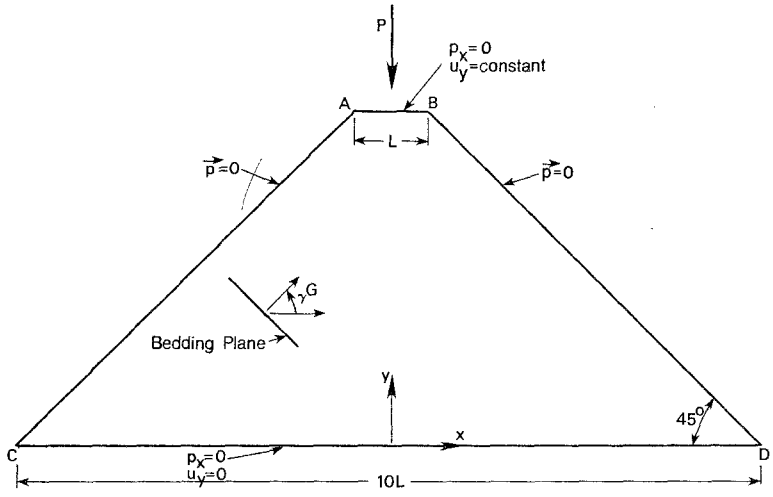

Fig. 2. Problem Geometry
Geometrie des Problems
Géométrie de problème

As P/L increases, fracture is initiated at surrounding points forming a growing region of damage. Each contour shown on Figs. 3—8 represents the value of P/L necessary to propagate the damage to that contour. Macrofracture, which forms the resultant chip, is assumed to propagate through this damage region following to a first approximation the minimum gradient of K [4, 5].

3. Numerical Results

The specific problem geometry is that shown in Fig. 2. This geometry has been chosen because of experimental convenience and comparison with currently available analytical and experimental isotropic solutions [2—5].

The problem solution is in two parts. The first part is the determination of the prefracture stress field. This is a linear isotropic elasticity problem. The boundary conditions are mixed, i. e.,

$$\begin{gathered} p_x = 0 \quad \text{on} \quad AB,\ BD,\ DC,\ CA \\ p_y = 0 \quad \text{on} \quad BD,\ CA \\ u_y = \frac{E\bar{u}_y}{P} = u_{y_0} \quad \text{on} \quad AB \\ u_y = 0 \quad \text{on} \quad DC \end{gathered} \tag{6}$$

where p_x, p_y, u_x, u_y are dimensionless traction and displacement components. The tractions have been nondimensionalized with respect to P/L and the displacements with respect to P/E. Note that the total line force P on AB and not the uniform displacement is the usual measured quantity. Computation of the fracture function, Eq. (5), requires a stress field due to a unit P/L. Thus, u_{y_0} represents the dimensionless displacement due to a unit P/L, which is unknown apriori. The difficulty is circumvented by assuming a unit uniform displacement, calculating the total line force by integrating the normal traction on AB resulting from the unit displacement, and then scaling the stresses to give a unit P/L, see [15]. An integral method which is particularly convenient for this problem has been used for stress field determination. This is outlined in detail for this problem in Ref. [15] and for brevity will be omitted here.

The material used to illustrate the analysis is a type of Green River Shale, for which the elastic constants[4] are [8]

$$E = 3.8 \times 10^4 \; MPa \qquad \nu = 0.2 \tag{7}$$

With the principal stresses (σ_1, σ_2) and principal directions, $(\alpha_1, \alpha_1 + \pi/2)$[5] known, the fracture analysis can be done. Eq. (5) is used directly to determine the global loading P/L necessary to initiate fracture (in the sense of coalescence of microcracks) at a given field point. The values of C, μ needed in Eq. (5) for this type of Green River Shale are [13]

$$C = \begin{cases} 73.8 - 29.6\ [\cos 2\ (\pi/6 - \gamma)]^6 & 0 \le \gamma \le \pi/6 \\ 60.7 - 16.5\ [\cos 2\ (\pi/6 - \gamma)]^6 & \pi/6 \le \gamma \le \pi/2 \end{cases} \qquad \mu = 0.589 \tag{8}$$

where the dimension of C is MPa. Note the isotropic character of μ.

Note that the angle γ in Eq. (8) (derived from experimental data) is defined only in the range $0 \le \gamma \le \pi/2$. To define γ, for use in Eq. (5), a global angle γ^G is introduced where γ^G is the angle measured from the x-axis to the normal to the bedding plane, $0 \le \gamma^G \le \pi$, see the inset of Fig. 2. In terms of γ^G and α_1, γ at a given field point is

$$\gamma = \begin{cases} -\gamma^G + \alpha_1, & -\pi/2 \le \gamma^G - \alpha_1 \le 0 \\ \gamma^G - \alpha_1, & 0 \le \gamma^G - \alpha_1 \le \pi/2 \\ \pi - \gamma^G + \alpha_1, & \pi/2 \le \gamma^G - \alpha_1 \le \pi \\ \gamma^G - \alpha_1 - \pi, & \pi \le \gamma^G - \alpha_1 \le 3\pi/2 \end{cases} \tag{9}$$

[4] Actually, slight elastic anisotropy was found in Ref. [8]. Ranges of various E's, ν's at zero confining pressure were

$$3.77 \times 10^4 < E < 3.85 \times 10^4$$
$$0.18 < \nu < 0.24$$

[5] α_1, is the angle measured from the x-axis to the direction of the maximum principal stress σ_1, $-\pi/2 \le \alpha_1 \le \pi/2$.

The fracture function $K=P/L$ is now computed at a selected grid of field points covering the suspected region of fracture initiation. Contour

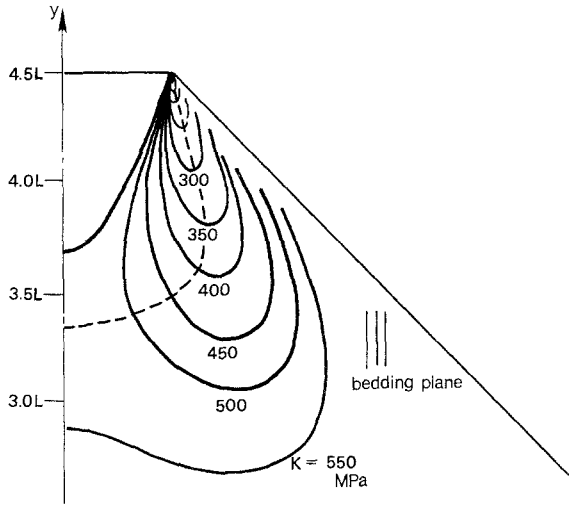

Fig. 3. Contour plot of fracture function for displacement of AB; $\gamma^G=0^0$
Konturkarte des Bruches für Verschiebung von AB; $\gamma^G=0^0$
Diagramme représentant la propagation des dommages produits par poussée de AB; $\gamma^G=0^0$

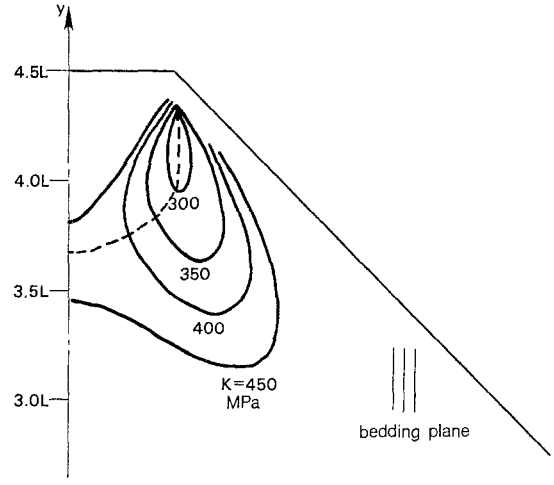

Fig. 4. Contour plot of fracture function for uniform traction on AB; $\gamma^G=0^0$
Konturkarte des Bruches für gleichförmiges Ziehen an AB; $\gamma^G=0^0$
Diagramme représentant la propagation des dommages produits par traction de AB; $\gamma^G=0^0$

plots of K can then be constructed by interpolation. Again, a given contour represents the global force level P/L necessary to propagate the damage region to that contour.

Figs. 3, 5 and 7 are contour plots for $\gamma^G=0$, $\pi/4$, $\pi/2$, respectively and for a prescribed uniform normal displacement on AB. Fracture initiates at

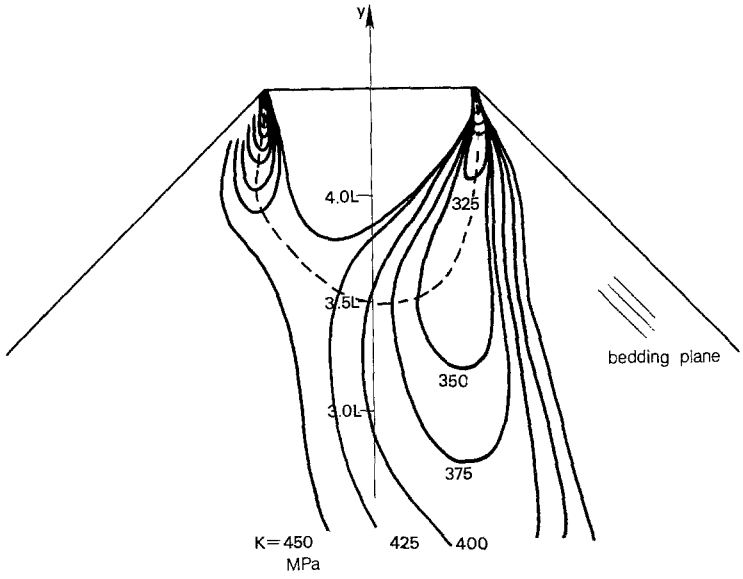

Fig. 5. Contour plot of fracture function for displacement of AB; $\gamma^G=45^0$
Konturkarte des Bruches für Verschiebung von AB; $\gamma^G=45^0$
Diagramme représentant la propagation des dommages produits par poussée de AB; $\gamma^G=45^0$

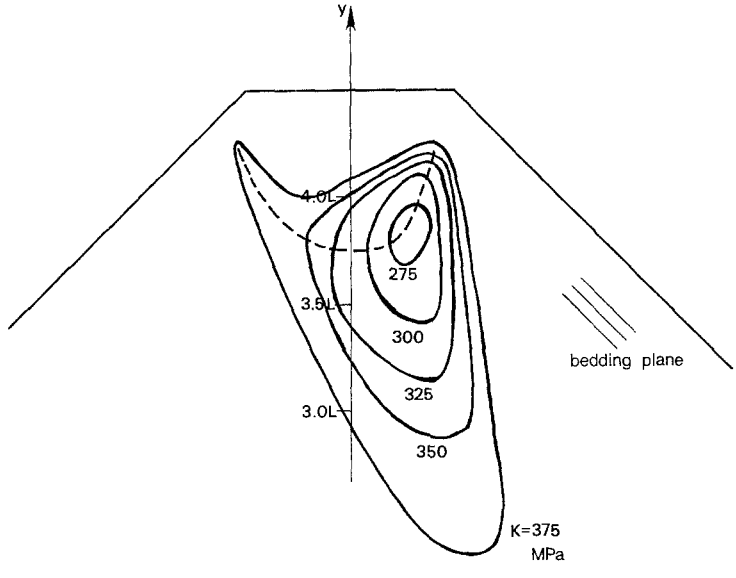

Fig. 6. Contour plot of fracture function for uniform traction on AB; $\gamma^G=45^0$
Konturkarte des Bruches für gleichförmiges Ziehen an AB; $\gamma^G=45^0$
Diagramme représentant la propagation des dommages produits par traction de AB; $\gamma^G=45^0$

the corners A, B (symmetrically for $\gamma^G = 0, \pi/2$) in all three cases due to the large stress gradients there, with the initial damage propagating vertically.

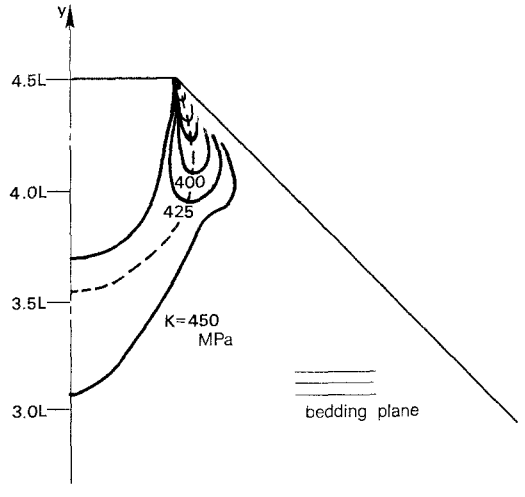

Fig. 7. Contour plot of fracture function for displacement of AB; $\gamma^G = 90^0$
Konturkarte des Bruches für Verschiebung von AB; $\gamma^G = 90^0$
Diagramme représentant la propagation des dommages produits par poussée de AB; $\gamma^G = 90^0$

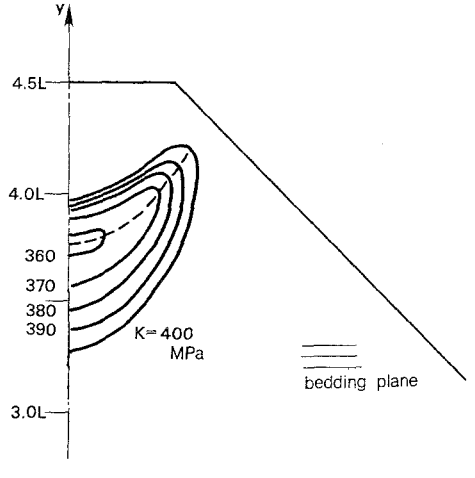

Fig. 8. Contour plot of fracture function for uniform traction on AB; $\gamma^G = 90^0$
Konturkarte des Bruches für gleichförmiges Ziehen an AB; $\gamma^G = 90^0$
Diagramme représentant la propagation des dommages produits par traction de AB; $\gamma^G = 90^0$

It is important to point out that the theory is accurate only for initiation and initial propagation since it neglects changes in material properties which occur in the damage region. This initial agreement is demonstrated in the

isotropic case in Ref. [5]. In an effort to provide a better estimate of the latter stages of damage growth, a second boundary condition was considered, namely a uniform normal traction on AB. This estimate is based on the initial damage propagating vertically, i. e., a uniform normal displacement on a rectangular geometry results in a uniform normal traction component. Figs. 4, 6 and 8 are the results of this computation for $\gamma^G = 0, \pi/4, \pi/2$, respectively. In all figures, dashed lines represent estimated macrofracture paths.

Estimates of fracture initiation loads, chip formation loads and chip depths are summarized in the table. Initiation loads for the displacement problems are estimated by K values at points as close to the corner as the numerics permit (0.25 L from the corner). Initiation begins internally in the uniform traction cases and loads are consistently higher than the initiation loads in the displacement problems. This was also the case in the isotropic results. The initiation load is lowest for the bedding plane vertical ($\gamma^G = 0$) and for $\gamma^G = \pi/4$ (45°), initiation is asymmetric. Both results are intuitively correct.

A new type of chip formation, not found in the isotropic case, is predicted by the displacement and traction solutions for $\gamma^G = \pi/4, \pi/2$. For these cases, fracture initiates at the corners. After a relatively small amount of damage growth, a new initiation site occurs internally. The chip is finally formed when the three damage regions join. Chip formation in the isotropic and $\gamma^G = 0$ cases occurs when the growing damage regions from both corners join. Chip formation loads are estimated by the intersection of common

Table 1. Numerical Results

γ^G (Degrees)		P_I/L Fracture initiation load (MPa)		P_F/L Approximate chip formation load (MPa)	Δ/L Approximate chip depth
0°	Displ.	78		520	1.1
	Trac.	270		420	0.75
45°	Displ.	A 105	B 95	440	1.0
	Trac.	260		370	0.85
90°	Displ.	105		430	1.0
	Trac.	350		390	0.75

damage contours. Results are similar to the isotropic results in that the traction chip formation load estimates are lower than the displacement. A questionably deep and skewed damage region is predicted for $\gamma^G = \pi/4$. A refined theory as well as some experimental data are needed to confirm the above predictions. Using the isotropic experimental results [5] as a guide we can expect that both the predicted chip formation loads and chip depth are too large.

4. Summary

A two dimensional, isotropic theory for the initiation and growth of damage regions in elastic brittle materials (rock) subjected to globally compressive stress fields has been extended to anisotropic fracture behavior. The specific anisotropy considered is of the "bedding plane" type, i. e., there is a preferred microcrack distribution parallel to the bedding plane. The theory defines damage as coalescence of propagating microcracks. The growth of this damage is described quantitatively by "fracture function" contours. Such contours were constructed for three cases; the bedding plane vertical ($\gamma^G = 0$), at 45° ($\gamma^G = \pi/4$), and horizontal ($\gamma^G = \pi/2$). Two different boundary conditions were investigated for each case. The prescribed displacement boundary condition provides accurate initiation and initial growth results while the prescribed traction boundary condition provides a better approximation of the latter stages of fracture growth. Chip shape for all cases as defined by the contours appear intuitively reasonable. Experimental results, similar to those done in the isotropic case, are needed for confirmation of the theory.

Appendix

Nonlinear, Anisotropic Fracture Analysis

Eq. (1):

$$|\bar{\tau}| + \mu(\gamma)\,\bar{\sigma} = C(\gamma) \tag{A-1}$$

describes a linear (Coulomb-Mohr) fracture envelope for material orientation, γ. While reasonable for some rock types, such a description is not valid in general. Fairhurst [16] has shown that the fracture behavior of a large class of rocks can be better represented by a nonlinear (Mohr) fracture envelope of parabolic form. In Ref. [17], a fracture function is derived, based on such a parabolic envelope, for isotropic rock. In this appendix, the extension to anisotropic rock is presented.

The parabolic Mohr Envelope for anisotropic rock is:

$$\begin{aligned} \bar{\tau}^2 &= [m(\gamma) - 1]^2\, S_t(\gamma)\, [S_t(\gamma) - \bar{\sigma}] \\ m(\gamma) &= \left[\frac{S_c(\gamma)}{S_t(\gamma)} + 1\right]^{1/2} \end{aligned} \tag{A-2}$$

where $S_c(\gamma)$, $S_t(\gamma)$ are the numerical values of the compressive and tensile strengths of the material at orientation, γ.

The state of stress at a given point in the field can be represented by a Mohr's circle in $\bar{\sigma} - \bar{\tau}$ space:

$$\left[\bar{\sigma} - \left(\frac{P}{L}\right)\frac{\sigma_1 + \sigma_2}{2}\right]^2 + \bar{\tau}^2 = \left[\left(\frac{P}{L}\right)\frac{\sigma_1 - \sigma_2}{2}\right]^2 \tag{A-3}$$

where σ_1, σ_2 have been nondimensionalized as in Eq. (5). Such a circle lies

inside the parabolic envelope and is tangent to it under the condition [17]:

$$\frac{P}{L}=K\ [\sigma_1,\ \sigma_2;\ S_t\ (\gamma),\ S_c\ (\gamma)]=\begin{cases}\dfrac{S_t(\gamma)\ [m\ (\gamma)-1]}{(\sigma_1-\sigma_2)^2}\{2\ [(\sigma_1-\sigma_2)^2 \\ \qquad +[m\ (\gamma)-1]^2\ \sigma_1\sigma_2]^{1/2} \\ \qquad -[m\ (\gamma)-1]\ (\sigma_1+\sigma_2)\} \\ \qquad \text{for } m(\gamma)\ [m(\gamma)-2]\,\sigma_1+\sigma_2<0 \\ \dfrac{S_t(\gamma)}{\sigma_1} \qquad \text{for } m(\gamma)\ [m(\gamma)-2]\,\sigma_1+\sigma_2\geq 0\end{cases} \tag{A-4}$$

The functions $S_t\ (\gamma)$, $S_c\ (\gamma)$ can be expressed as curve fits to experimental data of tests run for $0\leq\gamma\leq\pi/2$ and the analysis can proceed as in the linear case.

Acknowledgment

The authors gratefully acknowledge the support afforded by the National Science Foundation under Grant No. NSF GK-37289.

This paper was presented at the ASME Energy Technology Conference and Exhibition, Petroleum Division, Houston, Texas, September, 1977.

References

[1] Sikarskie, D. L., and J. B. Cheatham: Penetration Problems in Rock Mechanics. Rock Mechanics Symposium, AMD-Vol. *3*, ASME, 41—71 (1973).

[2] Altiero, N. J., and D. L. Sikarskie: Fracture Initiation in Elastic-Brittle Materials Having Nonlinear Fracture Envelopes. Intl. J. Fracture. Vol. *11*, No. 3 431—440 (1975).

[3] Sikarskie, D. L., and N. J. Altiero: The Formation of Chips in the Penetration of Elastic-Brittle Materials (Rock). J. Applied Mech., Vol. *40*, No. 3; Trans. ASME, Vol. *95*, 791—798 (1973).

[4] Altiero, N. J., and D. L. Sikarskie: Fracture Initiation and Propagation in Elastic-Brittle Materials Subjected to Compressive Stress Fields — An Experimental Study. Mech. Res. Comm., Vol. *1*, No. 4, 225—231 (1974).

[5] Altiero, N. J., and D. L. Sikarskie: Some Experimental Observations on the Initiation and Propagation of Fracture in Elastic-Brittle Materials Subjected to Compressive Stress Fields. Developments in Mechanics. Proc. of the 14th Midwestern Mechanics Conf. Vol. *8*, 155—170 (1975).

[6] Walsh, J. B., and W. F. Brace: Mechanics of Rock Deformation. Rock Mechanics Symposium, AMD-Vol. *3*, ASME, 1—24 (1973).

[7] Birch, F.: The Velocity of Compressional Waves in Rocks to 10 Kb., 2. J. Geophys. Res. Vol. *66*, 2199—2224 (1961).

[8] Podio, A. L., A. R. Gregory, and K. E. Gray: Dynamic Properties of Dry and Water-saturated Green River Shale under Stress. J. Soc. Pet. Engrs., Vol. *8*, No. 4, 389—404 (1968).

[9] Donath, F. A.: Strength Variation and Deformational Behavior of Anisotropic Rocks. In: State of Stress in the Earth's Crust. pp. 281—298. New York: American Elsevier Co. 1964.

[10] Jaeger, J. C.: Shear Failure of Anisotropic Rocks, Geological Magazine. Vol. *97*, 65—72 (1960).

[11] Walsh, J. B., and W. F. Brace: A Fracture Criterion for Brittle Anisotropic Rocks. J. Geophys. Res., Vol. *69*, No. 16, 3449—3456 (1964).

[12] Hoek, E.: Fracture of Anisotropic Rock. J. South African Inst. Min. and Met., Vol. *1*, No. 10, 510—518 (1964).

[13] McLamore, R., and K. E. Gray: The Mechanical Behavior of Anisotropic Sedimentary Rocks. Trans. ASME, Series B, Vol. *89*, 62—76 (1967).

[14] Kobayashi, S.: Fracture Criteria for Anisotropic Rocks, Kyoto Univ. Fac. Eng. Mem., Vol. *32*, Part 3, 307—333 (1970).

[15] Altiero, N. J., and D. L. Sikarskie: An Integral Equation Method Applied to Penetration Problems in Rock Mechanics. Boundary-Integral Equation Method: Computational Applications in Applied Mechanics, AMD-Vol. *11*, ASME, 119—141 (1975).

[16] Fairhurst, C.: On the Validity of the 'Brazilian' Test for Brittle Materials. Intl. J. Rock Mech. Min. Science, Vol. *1*, 535—546 (1964).

[17] Altiero, N. J.: On the Edge Fracture Problem of Rock Mechanics. Mechanics Research Communications. Vol. *3*, 345—352 (1976).

Addresses of the authors: N. J. Altiero, Department of Metallurgy, Mechanics and Materials Science, Michigan State University, East Lansing, Michigan; and D. L. Sikarskie, Department of Aerospace Engineering, The University of Michigan, Ann Arbor, Michigan, U. S. A.